7.805 CHARACTERIZATION OF THE EFFECTS OF CLOUD HETEROGENEITY ON CLOUD FRACTION AND CLOUD RADIATIVE EFFECTS

Clement Li
City College of the City University of New York, New York, NY
Stephen E. Schwartz
Brookhaven National Laboratory, Upton, NY
Viviana Vladutescu
New York City College of Technology, Brooklyn, NY
Antonio Aguirre
New York City College of Technology, Brooklyn, NY

ABSTRACT

Properties and extent of clouds have been examined by high resolution digital photography from the surface. High spatial resolution allows detailed examination of common measures of cloud contributions to atmospheric radiation; these cloud radiative effects exert major influences on Earth's radiation budget and thus must be accurately represented in climate models. The novel approach presented here makes use of a commercially available digital camera to quantify sky radiation in red, green, and blue channels with a spatial resolution (Rayleigh diffraction limit) of 30 µrad (30 mm at 1 km). Typical deployment is vertically pointing with field of view 22 x 29 mrad (~2 x 3 sun diameters). The camera's spectral response was characterized using an integrating sphere with a Mercury Xenon lamp source and monochromator and a photodiode with NIST-traceable calibration. The spectral and spatial response of the camera are used to calculate the cloudy and clear sky contributions to radiant intensity and the dependence of cloud areal fraction on threshold and resolution. Spatial variability is characterized by the power spectrum of the Fourier transform. Fractal dimension is determined by the slope of the power spectrum and by a box counting method.

Red and Blue intensities are found to be non-orthogonal measures of cloudy and clear-sky contribution to radiant intensity. The ratio RRB = Red/(Red + Blue), commonly used as a discriminant between cloud and clear sky, is high in cloudy regions and low in clear-sky regions. Values of RRB frequently exhibit a rather monomodal histogram rather than bimodal as would be expected for distinct regions of cloudy and clear sky. Cloud fraction determined from RRB is highly sensitive (several tens of percent) to the threshold and resolution. Principal component analysis shows that normalized Red and Blue intensities are accurately represented by a single component that is strongly correlated with RRB; thus RRB appears to be more useful as a measure of cloud contribution to radiance than as a discriminant. Cloud fractal dimension determined from RRB is found to differ substantially when determined by different methods, raising questions of the utility of this quantity to characterize cloud properties. These results demonstrate that cloud fraction cannot be uniquely defined or measured, raising question over the utility of this commonly used quantity.

Author addresses:
Clement Li, City College of the City University of New York, Department of Electrical Engineering, New York, NY 10031.
Email: cli14@citymail.cuny.edu
Stephen E. Schwartz, Brookhaven National Laboratory, Atmospheric Sciences Division, Upton NY, 11973.
Email: ses@bnl.gov
Viviana Vladutescu New York City College of Technology, Department of Electrical and Telecommunications Engineering Technology, Brooklyn NY 11201
Email: vvladutescu@citytech.cuny.edu
Antonio Aguirre, New York City College of Technology, Applied Mathematics, Brooklyn, NY 11201
Email: sadykov1@yahoo.com

1. INTRODUCTION

Clouds exert important influences on the shortwave and longwave radiation budget of the planet (Harrison et al., 1990). These effects must be accurately represented in climate models and hence must be accurately measured. Cloud effects are frequently represented in models, making use of cloud areal fraction, the fraction of a scene that contains clouds. Likewise, cloud fraction is commonly a measure of cloud amount in satellite measurements (King et al, 2013) and surface measurements (DOE, ARM, 1996). However, it is pointed out (e.g., DiGirolamo and Davies, 1997) that such

measurements are dependent on resolution and threshold. Likewise, determination of cloud fraction by multiple techniques results in highly differing values (several tens of percent) in comparisons with a variety of temporal averages (Wu et al., 2014). These studies raise question over the utility of cloud fraction as a measure of cloud amount or radiative effect. We, thus, undertook to examine cloud influence on radiation at high spatial resolution by surface based digital photography to systematically examine the dependence of cloud fraction on resolution and threshold. Alternative approaches to charactering cloud properties have also been examined. Preliminary findings are reported here.

	Fujifilm Finepix S1 digital camera specifications		
	Focal length = 215 mm , f# = 5.6, Effective aperture diameter = 38.4 mm, 35 mm Equivalent focal length = 1200 mm		
	Output: 3456 x 4608 pixels; 16 bit of red green and blue		
	λ = 450 nm	λ = 532 nm	λ = 650 nm
Rayleigh criterion, µrad (mm @ 1 km)	29	34	41
Pixel FOV, µrad (mm @1 km)	6.3		

Table 1: Comparison of Rayleigh Criterion of optics versus the field of view per pixel of the sensor for Fujifilm

2. CAMERA SPECIFICATIONS AND PROPERTIES

The camera used is a Fujifilm Finepix digital camera model S1; specifications are given in Table 1. The camera outputs RAW images that are converted to TIFF images with 22 x 29 mrad field of view in 3456 x 4608 pixels; each pixel provides 16 bit intensity data for red, green and blue channels, i.e., 0 – 65535 counts, in default gamma setting of 1.15. The camera is set to maximum focal length to observe clouds at a distance. At maximum focal length, the Rayleigh criterion, the minimum separation angle between two objects to distinctively differentiate those two objects, is 29, 34, and 41 µrad, respectively, for wavelengths 450, 532 and 650 nm, Table 1.

Actual resolution was examined by photographing a test pattern set up to view structure of 1, 2, 4 and 8 cm bars from a distance of 1 km, Figure 1 a and b. Analysis of line profile of the 4 cm bars showed that the bars were well resolved.

The camera's spectral response was calibrated by analyzing images recorded from a Mercury-Xenon lamp and monochromator emitting wavelengths from 300 to 800 nm in increments of 10 nm to a photodiode with NIST-traceable calibration, Figure 2. The central wavelengths for red, green and blue are found to be 614, 547 and 479 nm respectively. Red and blue exhibit little spectral overlap.

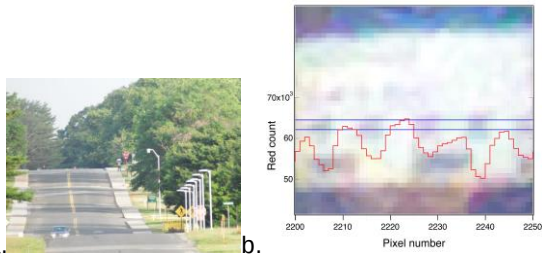

Figure 1: a. Set up of camera for the resolution test. b. Target at 1 km, line profile of red channel intensity over the 4 cm bars of target at 1 km. Note stop sign and individual holding test pattern.

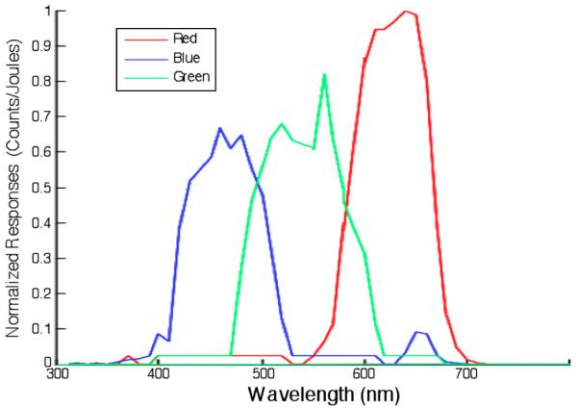

Figure 2: Spectral response of red, green and blue channels of the Fujifilm Finepix S1 digital camera.

Figure 3: Example of 28 photographs taken at 1 minute intervals on 07/29/2014 from 16:07 to 16:35. Image outlined in red is examined further in the analysis presented in sections 4 - 5.

3. EXAMPLES OF CLOUD PHOTOGRAPHS

The camera was set up to take photographs at one minute intervals; measurements were made at Upton, Long Island, New York (40.8694° N, 72.8867°) during daytime hours over a six week period in the summer of 2014. Very frequently, clouds exhibit high structure, even within the small area given by the camera field of view (roughly 2 x 3 sun diameters), Figure 3, which also displays the temporal variability often observed. The horizontal line profile of the cloud, Figure 4, demonstrates a greater variability in the red response when crossing from blue sky background to cloud than the blue response. This suggests the use of differences in intensity in the two channels as a measure of cloud contribution to observed radiance.

This structure exhibited at this resolution contrasts with the resolution of satellite products. For example, the standard MODIS satellite products have resolutions of 1 km or 250 m (Ackerman et al., 1998).

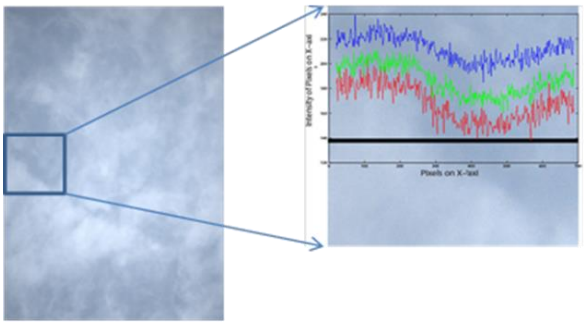

Figure 4: Red, green and blue response line profile upon the enlarged portion of a sample cloud image.

As a detailed example, we present a series of photographs, shown in Figure 5, at Upton, Long Island, NY, (07/29/2014 at 18:46, 20:01 and 20:16), together with ancillary data that allow determination of

additional cloud properties. A standard NOAA weather sonde, launched within 1 km from the observation site, showed close temperatures and dew point temperatures indicative of a thin, single layer cloud at 2.3 km, Figure 6, consistent with visual observations. An estimate of cloud optical thickness, COT, is obtained from a Cimel sky photometer (Cimel Electronique; www.cimel.fr; Chiu et al., 2012), Figure 7, indicating COT of 30, 35 and 5, respectively. Water vapor profile from a microwave radiometer provided cloud height throughout the course of 24 hours, Figure 8, showing an increased water vapor concentration during time period of the photographs. An image taken at 20:16 UTC, Figure 5c, was selected for detailed analysis because it exhibits a high degree of spatial variability. As the cloud in this image is at altitude 2.3 km, the image represents a spatial domain of 51 x 67 m.

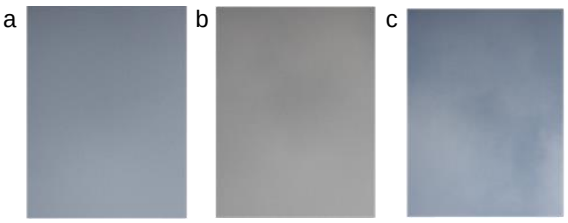

Figure 5: Three cloud images taken on July 29, 2014 obtained at times of retrievals of cloud optical thickness COT. a. 18:46 UTC b. 20:01 UTC c. 20:16 UTC with COT of 30, 35 and 5, respectively. c. image outlined red in Figure 3; further discussed in sections 4 - 5. Local standard time is UTC - 5 h.

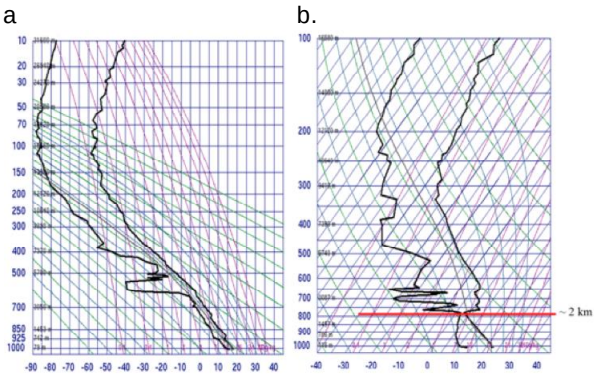

Figure 6: Radiosondes vertical profiles of temperature and dew point temperature; as measured by radiosondes launched above Brookhaven National Laboratory, Upton NY, 1 km from observation site at a. 00 UTC and b. 24 UTC on 07/29/2014. Close proximity of temperature and dew point temperature of radiosonde confirm single layer thin cloud at ~2 km at 24:00 UTC.

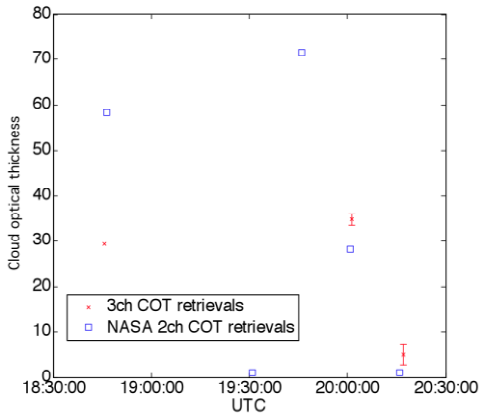

Figure 7: Cloud optical thickness (COT) retrievals from Cimel sun-sky photometer using the 2- and 3-channel retrieval methods (Chiu et al., 2012).

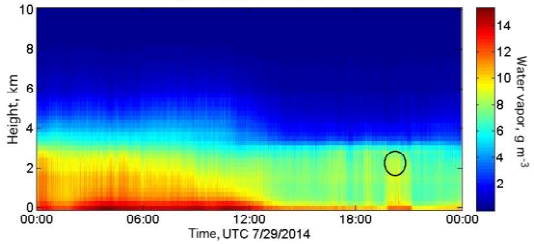

Figure 8: Vertical profiles of water vapor measured by microwave radiometer on July 29, 2014. High water vapor concentration shows clouds at ~2.5 km around 20 UTC indicated by the high water vapor concentration marked in circle.

4. CLOUD FRACTION

The effects of resolution and threshold on cloud fraction were examined for the cloud image shown in Figure 9. The histogram of the commonly used (Long et al., 2006) discriminant for clouds RRB = Red/(Red + Blue) is shown in Figure 10a and the cumulative distribution in Figure 10b. Here, as resolution is decreased, the value of RRB is evaluated from the means of red and blue intensities of the subpixels comprising the larger pixel; cloud fraction (CF) is defined as the fraction of pixels for which the RRB based on these ***average*** quantities exceeded the specified threshold. As threshold is increased the fraction of pixels exceeding the threshold decreases. Ultimately the cloud fraction for the entire image taken as a single pixel must become zero or unity. This analysis demonstrates that cloud fraction determined in this way is highly arbitrary, depending on the threshold and the resolution of the measurement, even at scales of a few meters. Such dependence of cloud fraction at scales well below those of current satellite observations raises questions about the interpretation of reported cloud fraction. Similarly, the variability of cloud amount over short spatial and

temporal scales raises question over the utility of cloud fraction as a means of representing the effects of clouds in climate models with grid cells of order 100 km, and the consequences of subgrid variability such as exhibited in the observations reported here.

Figure 9: Original natural color image from Figure 5 cropped to 3456 x 3456 pixels, used in analyses shown in Figures 10-12.

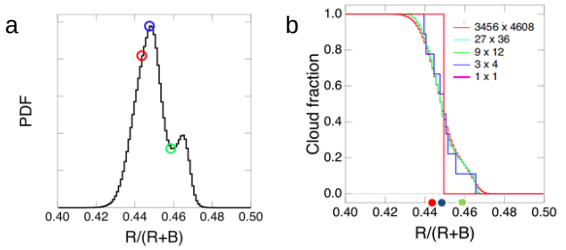

Figure 10: Probability density function and cloud fraction determined from RRB transform of image. Selected threshold points based on characteristics of PDF graph. Thresholds 0.4435, 0.4475, and 0.4585 used are indicated with red, blue and green circles respectively.

5. FRACTAL ANALYSIS

Fractal analysis is a widely used method of characterizing the complexity of objects (Kaperian, 2013; Green, 1998); fractional dimension is an index of how detail changes with resolution. There are multiple ways of determining fractal dimension. Here we present results obtained by the so-called box-counting method, where fractal dimension D is determined as

$$D = d \log C / d \log N$$

where N = number of boxes on a side of an image; (total number of boxes = N^2); C = number of boxes in which RRB exceeds the specified threshold value. Thus, the slope of a log-log plot of number of pixels meeting threshold criterion versus number of pixels on a side, yields the fractal dimension of an object, Figure 11.

Here, in contrast to the procedure of section 4, as resolution is degraded, a pixel is counted as "cloud" if any of the sub pixels contained any cloud (DiGirolamo and Davies, 1997). Hence, as resolution is degraded, CF approaches unity. However, as shown in Fig 12, for the counting algorithm, CF is highly dependent on the RRB threshold and resolution. At the highest resolution (1 pixel = 6 µrad = 12 mm at cloud height 2 km), CF can be as great as 0.72 with threshold RRB = 0.4435, and as low as 0.18 with threshold 0.4585. As resolution is degraded CF increases at all thresholds, because the larger pixels increasingly contain some cloud pixels. Ultimately, for the lower threshold values, for 9 pixels on a side (1 pixel = 2.3 mrad = 4.6 m), cloud fraction is unity for the two lower threshold values and 0.88 for the higher threshold.

Log-log plots shown in Figure 11a yield for the cloud image shown in Figure 9 fractal dimension D = 1.9, 1.8, and 1.7, respectively, as RRB threshold is taken as 0.4435, 0.4475, and 0.4585. Although this result might be viewed as showing only a weak dependence of D on threshold, as seen in Figure 12b, when the same data are plotted as *fraction* of pixels exceeding threshold vs number of pixels on a side (log-log plot), the slopes are quite different. The slopes in the two plots differ by exactly 2, a consequence of the alternative means of plotting. From this examination, it is seen that the fractal dimension of cloud fraction determined in this way, like cloud fraction itself, depends strongly on threshold and thus cannot be uniquely defined or measured.

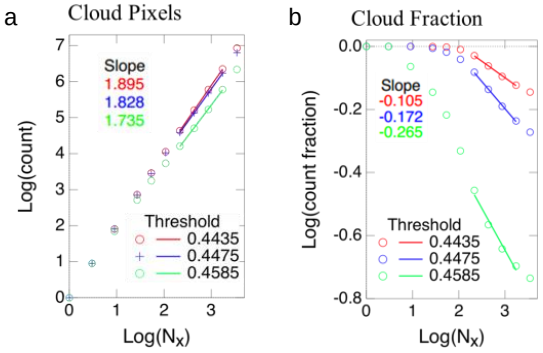

Figure 11: Fractal analysis of the cloud image in Figure 9. a. finds the fractal dimensions of cloud pixels. Here the y axis represents the Log of number of pixels that for which RRB exceeds the indicated threshold (colors as in Figure 10) versus log of the number of pixels on side of box (inverse of linear dimension). b. as in a, but for fraction of pixels that exceed threshold.

Method	Threshold	Slope	Uncertainty
Box counting	0.4435	1.895	0.003
	0.4475	1.828	0.005
	0.4585	1.735	0.029
Fractional area	0.4435	-0.105	0.003
	0.4475	-0.172	0.005
	0.4585	-0.265	0.029

Table 2: Conventional box-counting method versus fractional method. Uncertainties are same for either method. Both methods are equivalent.

.

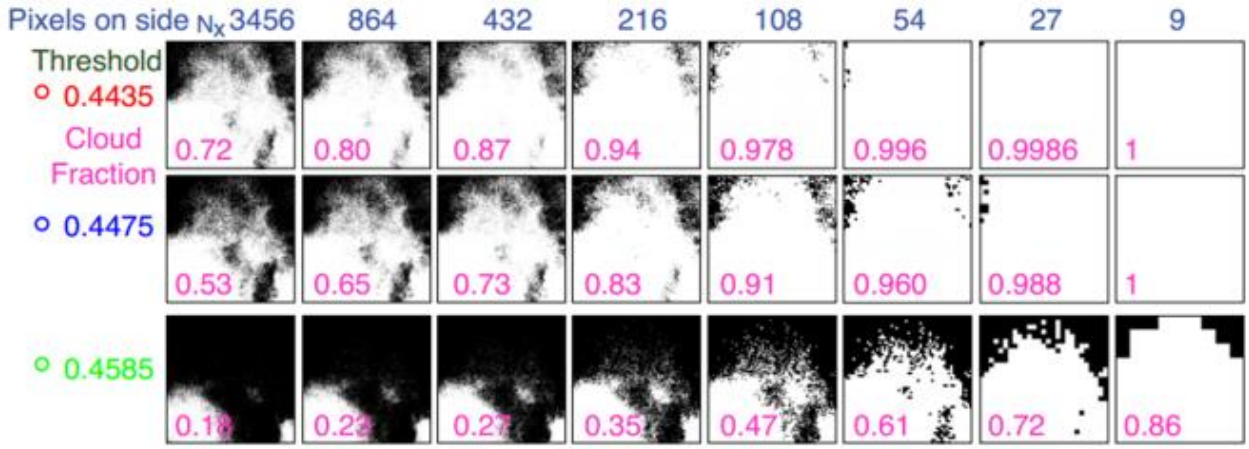

Figure 12: Dependence of cloud fraction of Figure 9 photograph on resolution and threshold, for counting algorithm such that a pixel is counted as cloud if any sub pixels contain cloud at the stated threshold level. Blue numbers at top give number of pixels on side, resolution decreasing to the right; colored numbers at left give threshold values corresponding to values shown in Figure 10, increasing top to bottom; magenta numbers give corresponding cloud fraction.

6. PRINCIPAL COMPONENT ANALYSIS

Principal component analysis was examined as a means of attributing the signal in a given subregion of the image to cloud versus cloud-free sky. Principal component analysis identifies orthogonal basis vectors that are linear combinations of measured quantities to permit description of measured quantities in terms of a reduced set of variables. The procedure developed here is illustrated with reference to Figure 13, which utilizes a pixelated image, *g,* created from the original image shown in *f*. As signal counts in the three channels were highly correlated, a measure of scene brightness, this correlation was accounted for by normalizing red and blue intensities, *a*, to green, *b*, and subtracting the means, *c*. By matrix diagonalization these quantities were expressed as a linear combination of two variables, e, in which almost all of the variance, 99.66% in this instance, was accounted for by a single variable that is a measure of whiteness-blueness of the image. This principal component is shown by the red lines in *h*, where the vertical location of the line in each pixel denotes the value of this component on a scale of -0.3 to + 0.3. Reversing the procedure to obtain the original RGB values of the individual pixels from only the principal component and the green intensity yields the reconstructed image, *i* which appears virtually identical to the original pixelated image *g*. The difference between the two images, shown on the same intensity scale, *j* is very close to zero (black). Multiplying that difference by 100, *k,* manifests the differences along the green-magenta axis, orthogonal to the blue-white axis (first principal component) that is a measure of the cloud contribution to the measured radiance. Finally, in *e*, the first principal component is shown to be highly correlated to the variable RRB, Red/(Red + Blue), commonly employed for cloud discrimination. Thus, it seems that RRB might usefully be employed as a measure of cloud contribution to radiance rather than a discriminant of cloud presence/absence. A further point to be noted in *h* is that despite the pixels in the upper right of the figure being much darker than those at the upper left of the figure, the first principal component remains very close to its maximum value; this indicates that this measure of cloud contribution to radiant intensity is only weakly dependent on pixel brightness. This lends strength to the interpretation of the first principal component, and by extension RRB, as a measure of cloud contribution to the radiance of a given pixel.

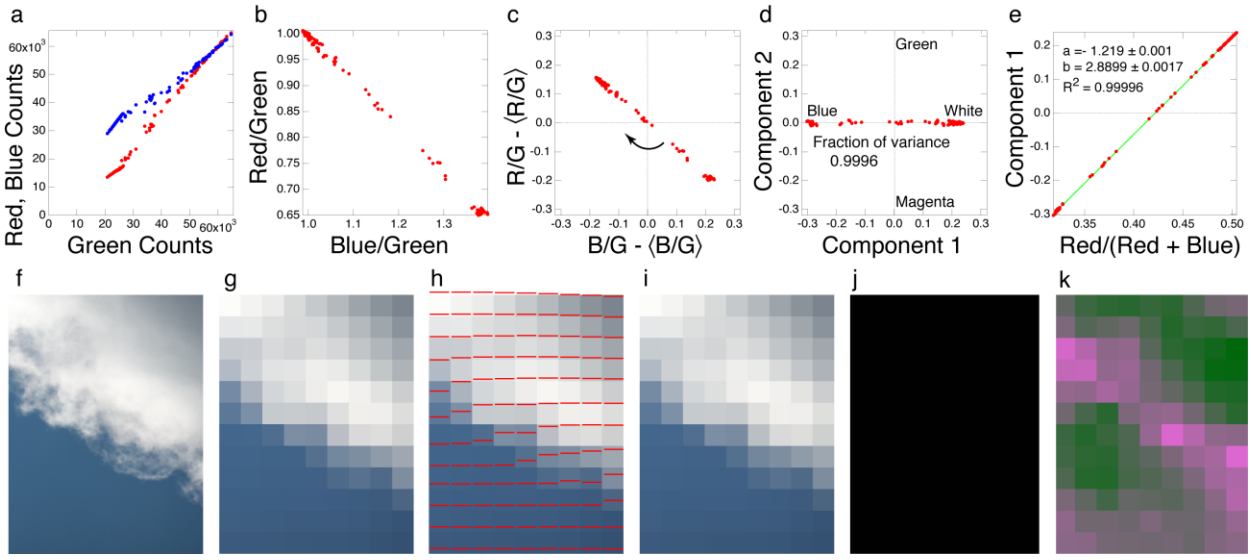

Figure 13: Principal component analysis of cloud contribution to radiant intensity. *a*. Intensity counts from pixelated digital image (*g*), Red (R) and Blue (B) versus Green (G); *b*. R/G versus B/G; *c*. normalized and mean-subtracted R/G versus B/G; *d*. data in *c* rotated to show two principal components; *e*. principal component 1 versus R/(R+B); *f*. original image; *g*, pixelated to 9 x 12; *h*; same as *g*, with principal component 1 superimposed; vertical scale of each box from -0.3 to 0.3; *i*, reconstruction of image using only principal component 1 and green intensity; *j*, difference of images i - g, on same intensity scale; *k* as *j*, but with intensity scale multiplied by 100.

7. CONCLUSION

Surface-based high resolution photography provides a new and highly detailed view of clouds at spatial resolution of a few centimeters, 4 to 5 orders of magnitude finer than satellite products. Even at such fine scales, cloud contribution to measured zenith radiance exhibits considerable structure. Cloud fraction inherently depends on threshold and resolution and therefore cannot be uniquely defined or measured. For a fixed resolution, as threshold is decreased, cloud fraction tends to increase if the threshold is below the mean, and vice versa. Examination of cloud fractal dimension by the commonly used box-counting method similarly showed dependence on threshold. Principal component analysis was able to represent the cloud and cloud-free sky contributions to measured radiance in terms of an overall intensity and a single color component and may lead to a robust means of quantifying cloud contributions to radiance

Acknowledgments. We thank Dong Huang, Laurie Gregory, Rick Wagener, Ivan Kotov, Peter Takacs, Mary Jane Bartholomew, all of BNL, for helpful discussions. Supported in part by the U.S. Department of Energy, Office of Science, Office of Workforce Development for Teachers and Scientists (WDTS) under the Visiting Faculty Program (VFP) and in part by the U.S. Department of Energy's Atmospheric Science Program (Office of Science, OBER) under Contracts. DE-AC02-98CH10886 and DE-SC00112704.

REFERENCES

Ackerman S. A., K. I. Strabala, W. P. Menzel, R. A. Frey, C. C. Moeller, and L. E. Gumley, Discriminating clear sky from clouds with MODIS. *J. Geophys. Res.*, **103**, 32141-32157 (1998).

Chiu, J. C., A. Marshak, C. H. Huang, T. Várnai, R. J. Hogan, D. M. Giles, B. N. Holben, E. J. O'connor, Y. Knyazikhin, and W. J. Wiscombe. Cloud Droplet Size and Liquid Water Path Retrievals from Zenith Radiance Measurements: Examples from the Atmospheric Radiation Measurement Program and the Aerosol Robotic Network. *Atm. Chem. Phys.* **12**, 10313-0329 (2012). .

Daftlogic Distance Calculator. http://www.daftlogic.com/projects-google-maps-distance-calculator.htm Last updated 16 October 2014.

Di Girolamo, L., & R. Davies. Cloud fraction errors caused by finite resolution measurements. *J. Geophys. Res.* **102**, 1739-1756 (1997).

Green, E. (1998) "Welcome to an Exploration of Fractals!" University of Wisconsin-Madison, 1998, http://pages.cs.wisc.edu/~ergreen/honors_thesis/Accessed 14 Jan. 2015.

Gueymard, C. A. The Sun's Total and Spectral Irradiance for Solar Energy Applications and Solar

Radiation Models. *Solar Energy* **76**, 423-453 (2004).

Harrison, E. F., P. Minnis, B. R. Barkstrom, V. Ramanathan, R. D. Cess, and G. G. Gibson. Seasonal Variation of Cloud Radiative Forcing Derived from the Earth Radiation Budget Experiment. *J. Geophys. Res.* **95**, 687-703 (1990).

Karperien, A. (2013) FracLac for ImageJ. http://rsb.info.nih.gov/ij/plugins/fraclac/FLHelp/Introduction.htm.

King, M. D., S. Platnick, W. P. Menzel, S. A. Ackerman, and P. A. Hubanks. Spatial and Temporal Distribution of Clouds Observed by MODIS Onboard the Terra and Aqua Satellites. *IEEE Trans. Geosci. and Rem. Sens.* **51**, 3826-3852 (2013).

Liu, Y., W. Wu, M. P. Jensen, and T. Toto. Relationship between Cloud Radiative Forcing, Cloud Fraction and Cloud Albedo, and New Surface-based Approach for Determining Cloud Albedo. *Atm. Chem. Phys.* **11**, 7155-7170 (2011).

Long, C. N., Sabburg, J. M., Calbó, J., & Pagès, D. Retrieving cloud characteristics from ground-based daytime color all-sky images. *J. Atmos. Oceanic Tech*. **23**, 633-652 (2006).

Wu, W., Y. Liu, M. P. Jensen, T. Toto, M. J. Foster, and C. N. Long (2014), A comparison of multiscale variations of decade-long cloud fractions from six different platforms over the Southern Great Plains in the United States, *J. Geophys. Res. Atmos*. **119**, 3438–3459.